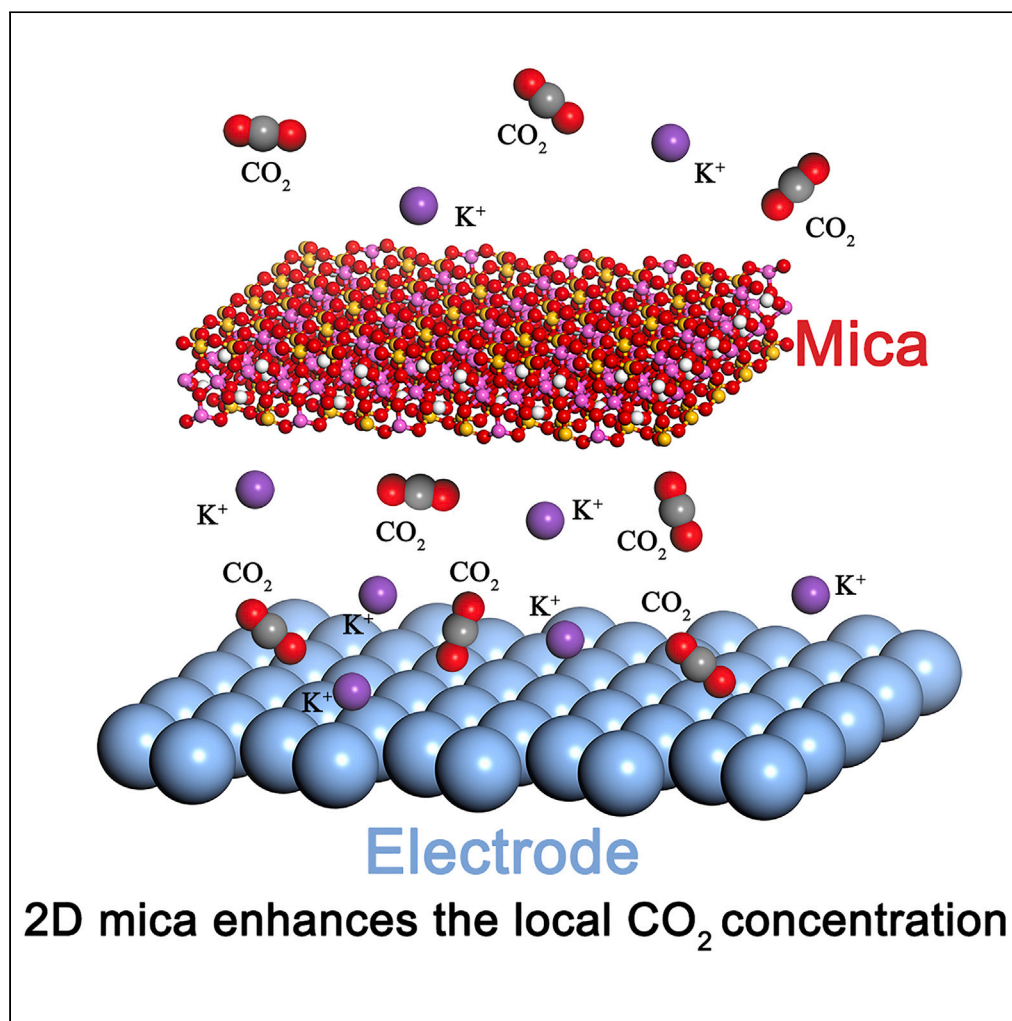


Article

Boosting CO₂ electrocatalysis through electrical double layer regulations

Qun Fan, Guangxu Bao, Hai Liu, ..., Peng Kang, Sheng Zhang, Xinbin Ma

sheng.zhang@tju.edu.cn

Highlights

Two-dimensional mica flakes modulate the electric double layer in CO₂ electroreduction

The high electrical double layer capacitance facilitates local CO₂ enrichment

Enriched local CO₂ concentration favors CO₂ electroreduction

Article

Boosting CO₂ electrocatalysis through electrical double layer regulations

Qun Fan,¹ Guangxu Bao,¹ Hai Liu,^{1,3} Yihan Xu,¹ Xiaoyi Chen,¹ Xiangrui Zhang,¹ Kai Li,¹ Peng Kang,¹ Sheng Zhang,^{1,2,4,*} and Xinbin Ma^{1,2}

SUMMARY

Interfacial investigation for fine-tuning microenvironment has recently emerged as a promising method to optimize the electrochemical CO₂ reduction system. The electrical double layer located at the electrode-electrolyte interface presents a particularly significant impact on electrochemical reactions. However, its effect on the activity and selectivity of CO₂ electrocatalysis remains poorly understood. Here, we utilized two-dimensional mica flakes, a material with a high dielectric constant, to modify the electrical double layer of Ag nanoparticles. This modification resulted in a significant enhancement of current densities for CO₂ reduction and an impressive Faradaic efficiency of 98% for CO production. Our mechanistic investigations suggest that the enhancement of the electrical double layer capacitance through mica modification enriched local CO₂ concentration near the reaction interface, thus facilitating CO₂ electroreduction.

INTRODUCTION

The electrochemical route of converting CO₂ into valuable chemical raw materials contributes to remediate anthropogenic greenhouse gas emissions and enhances the storage of intermittent renewable energy.^{1–4} Since the 1980s, electrocatalysts for CO₂ electrochemical reduction have undergone rapid development in terms of morphology and composition, which created favorable electronic structures to maintain high selectivity and activity.^{5–11} Tailoring microenvironment at solid-liquid interface has emerged in recent years toward a full optimization of the electrochemical systems, going beyond the catalyst's electronic structure. However, it is still challenging to completely comprehend the local reaction environment in such electrocatalytic systems.^{12–14}

The electrical double layer is located at the interface between electrode and bulk electrolyte, consisting of the Helmholtz plane and the diffusion layer. The Helmholtz plane is divided into inner Helmholtz plane, where ions and molecules are specifically adsorbed to the electrode surface, and the outer Helmholtz plane, defined as the nearest plane of solvated ions that are drawn to the electrode via electrostatic force.^{15,16} The diffusion layer is composed of loosely stacked layers of anions and cations, ensuring charge neutrality across the double layer and accounting for the exponential decrease in potential away from the electrode.¹⁷ Numerous theories propose that the electrical double layer plays a crucial role in migration, diffusion, and reaction process.^{18,19} For example, modulating electric field distribution in the double layer by alkali cations can impede the hydrogen evolution reaction by inhibiting the migration of protons.²⁰ Electrostatic interactions and proton/water dynamics in the electrical double layer also have been proposed to contribute to the of other electrochemical reactions.^{21,22} Currently, most of the regulation of the electrical double layer is relied on customizing the electrolyte; however, the effect of electrolyte is very complex and challenging to ascribe. Cations can stabilize *CO₂⁻ anionic radicals and reduce charge transfer resistance, enabling higher current densities at the same potential.^{23,24} Additionally, cations have been considered to provide enhanced buffering capacity, maintain a lower pH, and allow for a high concentration of locally dissolved CO₂.²⁵ Anions, such as halogenated elements, can specifically adsorb onto the cathode, transferring charge to metal catalytic site and thus altering the selectivity of CO₂ electroreduction reaction (CO₂RR).²⁴ Therefore, in order to gain a clear understanding of the effect of the electric double layer on the reaction, new systems need to be developed for further study.

Herein, two-dimensional mica flakes have been utilized to modulate the electric double layer of Ag nanoparticles, which is a typical catalyst for CO₂RR. Mica is a widely used dielectric material with excellent chemical stability, which enables it to withstand local alkaline environments close to the catalytic sites. Two-dimensional mica with nanometer thickness can inset on the electric double layer, ranging from Å to μm. By modification of mica flakes, the CO Faraday efficiency of Ag nanoparticles can reach an impressive 98% and the current density can be significantly improved. The calculations of the electric double layer capacitance reveal that the capacitance value of the mica flake modification was increased to 2.4 times that of the pre-modification, and *in situ* attenuated total reflection infrared absorption

¹Key Laboratory for Green Chemical Technology of Ministry of Education, Collaborative Innovation Centre of Chemical Science and Engineering, School of Chemical Engineering and Technology, Tianjin University, Tianjin 300072, China

²Haihe Laboratory of Sustainable Chemical Transformations, Tianjin 300192, China

³School of Chemistry and Chemical Engineering, Yancheng Institute of Technology, Yancheng 224051, China

⁴Lead contact

*Correspondence: sheng.zhang@tju.edu.cn

<https://doi.org/10.1016/j.isci.2024.109060>



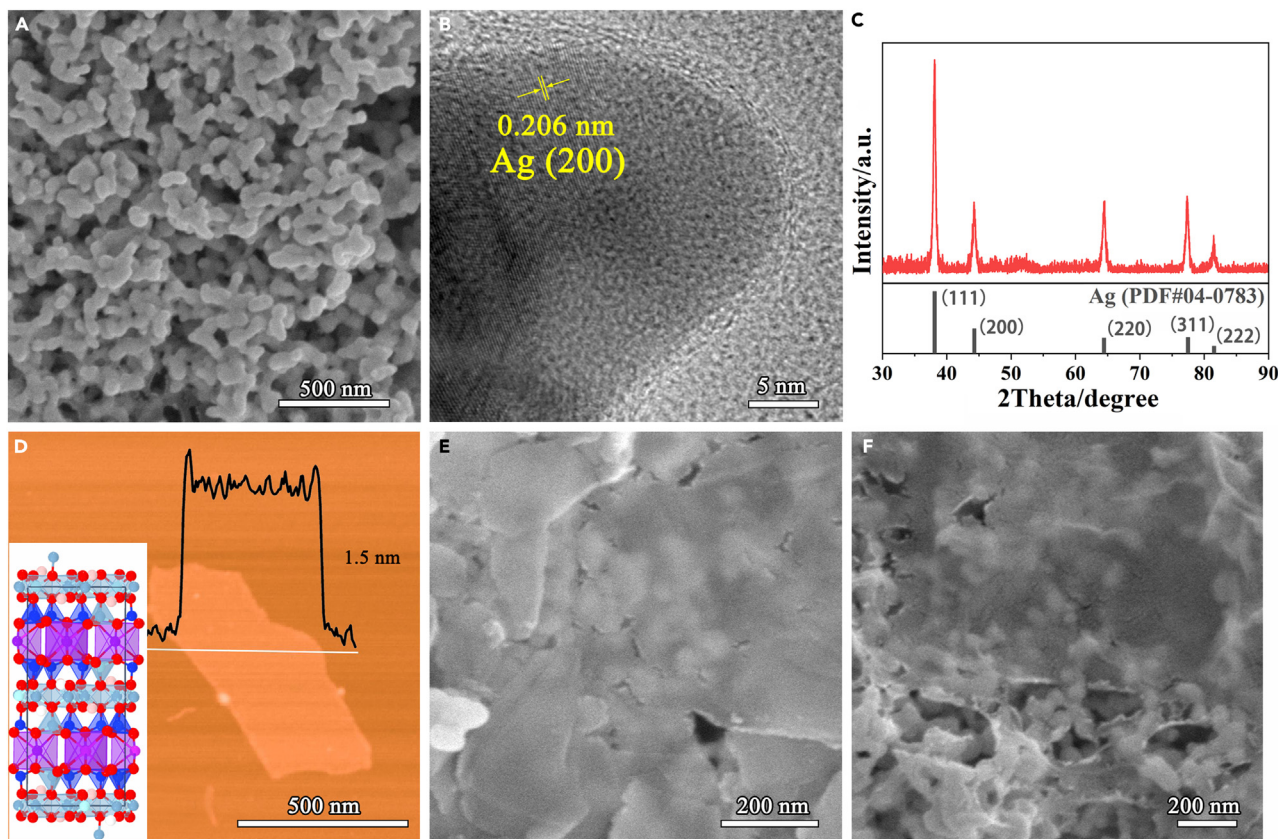


Figure 1. physical characterizations of Ag nanoparticles, mica flakes, Ag-mica, and Ag-graphene

(A) SEM image, (B) TEM image, and (C) XRD patterns of Ag nanoparticles.

(D) AFM image of mica flakes (The inset picture is the crystal structure of mica. K, Al, Si, H, and O are displayed, respectively, in purple, light blue, navy, pink, and red.).

(E) SEM image of Ag-mica.

(F) SEM image of Ag-graphene.

spectra demonstrate that the presence of mica flakes enhances the local CO_2 concentration at the electrode. These findings from the catalytic model suggest that the enhanced capacitance of the electric double layer can enrich the local CO_2 concentration, thereby enhancing electrocatalytic activity.

RESULTS AND DISCUSSIONS

Materials synthesis and characterizations

Ag nanoparticles were synthesized by a simple liquid phase reduction method. Sodium borohydride was used as a reducing agent to reduce Ag^+ , while sodium citrate was used as a stabilizer for the synthesis to help control the size of Ag nanoparticles. Electron microscopy was used to characterize the microstructure of Ag nanoparticles. As shown in Figure 1A, the scanning electron microscope (SEM) image indicates that the synthesized Ag is in the form of particles with tens of nanometers size distribution. The Ag nanoparticles in the high-resolution transmission electron microscopy (TEM) image have obvious lattice stripes of Ag (Figure 1B). Their lattice spacing is 0.206 nm, which corresponds to the (200) crystal plane of Ag. The powder X-ray diffraction (XRD) patterns reflect Ag nanoparticles crystallize in the cubic $Fm\bar{3}m$ space group (JCPDS No. 04-0783). The typical diffraction peaks of 38.1° , 44.3° , 64.4° , 77.5° , and 81.5° can be ascribed to (111), (200), (220), (311), and (222), respectively. The grain size was calculated by Scherrer's formula to be 21.4 nm, which is similar to the size observed by electron microscopy.

Mica, a crystal with a layered structure in the monoclinic crystal system, is an aluminosilicate of metals such as potassium and aluminum, with chemical formula as $\text{KAl}_2(\text{AlSi}_3\text{O}_{10})(\text{OH})_2$ (the inset picture of Figure 1D). Due to the weak bonding between potassium ions and aluminosilicate layers, mica can be exfoliated perfectly along the (001) plane.²⁶ SEM images of bulk mica and mica flakes after ions exchange-assisted liquid phase exfoliation are shown in Figure S1. The images reveal that pristine layered mica has a micron plane size with a relatively flat surface. After exfoliation, the longitudinal size becomes thinner and it begins to exhibit a flake-like structure. Their thickness was measured by atomic force microscopy (AFM) to be several nanometers, presenting the few-layers nature of mica (Figure 1D).²⁷ Furthermore, prolonged

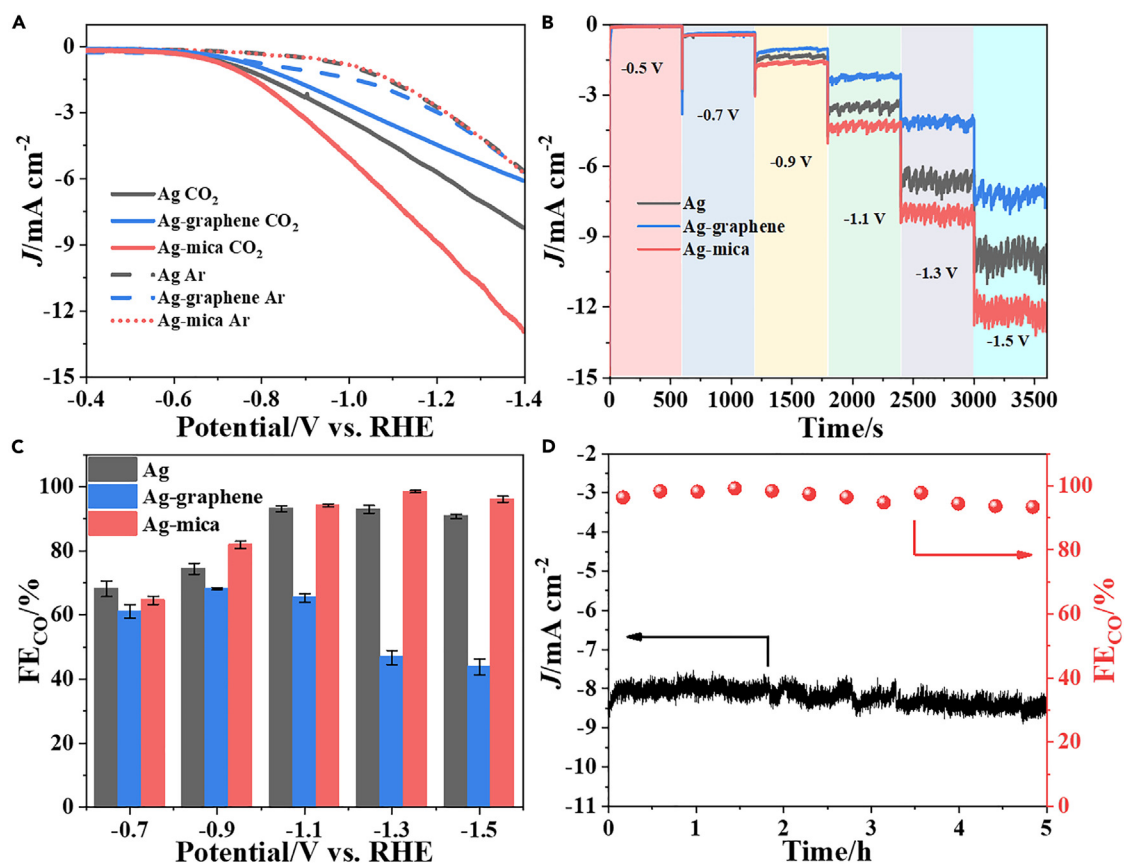


Figure 2. Electrocatalytic CO₂ reduction performance

(A) LSV curves of Ag nanoparticles, Ag-graphene, and Ag-mica in CO₂ or Ar-saturated 0.1 M KHCO₃ at a scan rate of 100 mV/s.

(B) Current density curves and (C) Faradaic efficiencies of Ag nanoparticles, Ag-graphene, and Ag-mica in CO₂-saturated 0.1 M KHCO₃ at applied potentials (The error bars represent two repeated electrolysis with different batches of catalysts).

(D) Stability of the Ag-mica in CO₂-saturated 0.1 M KHCO₃ at a potential of -1.3 V vs. RHE.

stirring and ultrasonication not only exfoliate mica from the longitudinal direction but also cause damage and fragmentation to the plane with size ranges approximately between one or two micrometers and tens of nanometers (Figures S1 and S2). In addition, mica is chemically stable and has a high dielectric constant,²⁸ making it an excellent class of dielectric material to modify Ag nanoparticles. SEM image of mica flakes-modified Ag nanoparticles (Ag-mica) is shown in Figure 1E. Due to the thin thickness, Ag nanoparticles under two-dimensional mica flakes could distinctly appear. As for contrast, graphene has also been utilized to modify Ag nanoparticles (Figure 1F).

CO₂RR performance

The CO₂RR activities were evaluated in a gas-tight three-electrode electrochemical configuration. Figure 2A shows the linear sweep voltammetry (LSV) measurements of Ag nanoparticles, Ag-graphene, and Ag-mica in 0.1 M KHCO₃ solution saturated with CO₂ or Ar. Under CO₂ condition, Ag-mica exhibited significantly higher current densities than pristine Ag nanoparticles, while Ag-graphene showed suppressed current densities relative to Ag nanoparticles. These results suggest that mica modification facilitated CO₂RR activity and graphene modification hindered the reaction. The onset potentials for the three specimens are similar due to the same Ag catalytic center. In an Ar atmosphere, both specimens experienced noticeable declines in current densities and onset potentials, revealing their intrinsic activities for CO₂ reduction.

To identify the reduction products, the controlled potential electrolysis was carried out for the three specimens. The gas-phase products were detected by the gas chromatograph, and the liquid products were analyzed through nuclear magnetic resonance. The analysis revealed that only CO and H₂ were detected as gaseous products, and no liquid phase products were observed. Mica flakes and graphene were also tested individually, and both showed hydrogen as the sole reduction product, with no carbon-containing compounds generated. Additionally, the reaction current densities for mica and graphene alone were found to be very low (Figure S3), indicating their inactivity for CO₂RR without the presence of Ag nanoparticles. As implied in Figure 2B, the current densities of Ag-mica were approximately 1.2 times those of Ag nanoparticles, while Ag-graphene had 5%–40% decrease in current densities compared to Ag nanoparticles. These results are

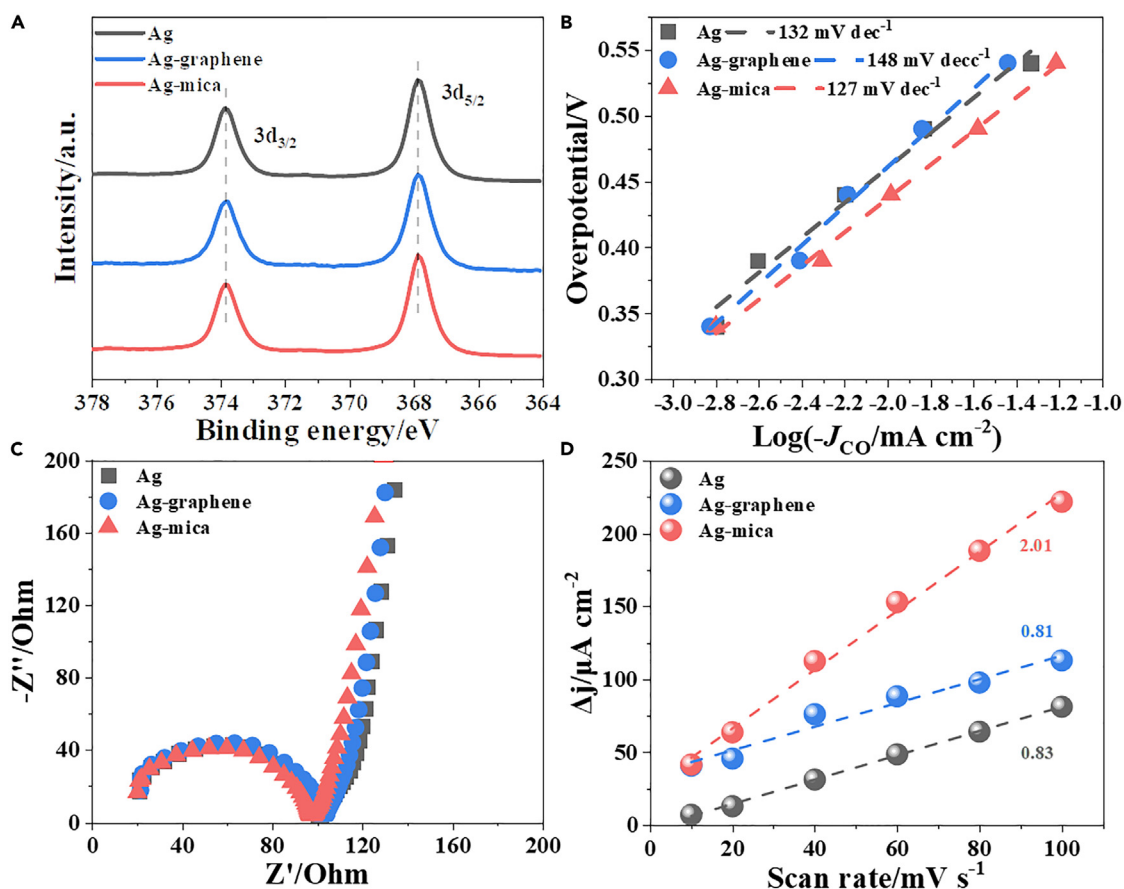


Figure 3. Mechanistic study

(A) XPS spectra of Ag 3d, (B) Tafel plots for CO₂RR to CO, (C) Nyquist plots, and (D) charging current density difference plotted against scan rate for Ag, Ag-graphene, and Ag-mica.

consistent with the trends observed in the LSV curves. The presence of graphene may partially cover the catalytic active sites of Ag or impede the mass transfer of reactants, leading to the descent of current densities. The CO Faradaic efficiencies of Ag-graphene were comparable to those of pristine Ag nanoparticles at lower potentials. However, at higher potentials, there was a significant drop in CO Faradaic efficiency, falling below 50%. This could be attributed to the fact that the Ag electrode surface covered with graphene restricts the mass transfer of CO₂, thereby reducing selectivity at high currents. On the other hand, the mica flake modification resulted in a slight increase in CO Faradaic efficiency compared to Ag nanoparticles, with a maximum value reaching up to 98%. The enhancements of CO Faradaic efficiency ranged 1%–7% for mica flake modification under different potentials. To assess the stability of Ag-mica, long-term chronoamperometry was conducted at -1.3 V vs. reversible hydrogen electrode (RHE). As depicted in Figure 2D, both the current density and the Faradaic efficiency of CO showed no significant decrease over 5 h of electrolysis, indicating the favorable stability of Ag-mica. After electrolysis, the microstructure and crystal structure of Ag-mica did not change (Figures S4 and S5).

Mechanism investigations

To further reveal the role of mica, a series of experiments were conducted. Firstly, X-ray photoelectron spectroscopy (XPS) and Auger electron spectroscopy were employed to investigate whether the modification of graphene and mica flakes impacts the electronic density of states of Ag. As depicted in Figure 3A, the binding energy remains unchanged after the modification with graphene and mica flakes. This suggests that there is no significant interaction between graphene and mica flakes on Ag nanoparticles that alters the electronic state density of Ag. Another batch of samples also displayed the same consequence (Figure S7). Therefore, the change in CO₂ electrochemical reduction performance is not attributed to the alteration of Ag electronic state.

Figure 3B illustrates the Tafel slopes of Ag nanoparticles, Ag-graphene, and Ag-mica, with the values of 132, 148, and 127 mV dec⁻¹, respectively. At low overpotentials in the Tafel slopes, when the reaction is just initiating, reaction is less influenced by mass transfer and mainly governed by electrochemical polarization. The similarity in Tafel slopes among the three specimens indicates that the modification does not affect electrochemical polarization resistance, and increasing the overpotential has a similar effect on the current density. Hence,

it can be inferred that graphene and mica flake modification does not alter the intrinsic catalytic activity of Ag nanoparticles. Instead, the modification primarily affects concentration polarization, specifically affecting the mass transfer process. In addition, the Tafel slope being close to 118 mV dec^{-1} suggests that the rate-determining step of the reaction is the first electron transfer to CO_2 , leading to the formation of CO_2^- . In Figure 3C, the Nyquist curves of Ag nanoparticles, Ag-graphene, and Ag-mica are shown. It is evident that the charge transfer impedance is similar for all three samples. This indicates that the modification did not affect the rate of charge transfer from Ag nanoparticles to reactants or intermediates.

When an electrocatalytic reaction occurs, charged particles in the solution converge toward the surface of the electrode due to electrostatic forces, which results in the electric double layer at the interface. The electric double layer can be approximated as a flat plate capacitor (Helmholtz model). According to the capacitance Equation 1, when the area opposite to the capacitor pole plate and the distance between the pole plates remain constant, a higher dielectric constant results in a higher capacitance value. Therefore, the high dielectric constant of mica theoretically enhances the capacitance value of the electric double layer. Furthermore, according to Equation 2, a higher capacitance corresponds to a greater charge carried in the electric double layer, assuming a constant voltage applied to the electrode surface. The charge exists in the form of electrons at the electrode and cations in the electrolyte. In our reaction system, cations are mainly the K^+ ions. Thus, the higher charge indicates a higher concentration of K^+ ions in the electric double layer. It has been reported that a high concentration of K^+ ions increases the local concentration of CO_2 at the electrode and lowers the energy barrier for CO_2 reduction, thereby enhancing reactivity.^{29,30} Additionally, mica is known to be rich in mobile K^+ ions. When mica flakes are modified on the electrode surface, they themselves can increase the concentration of K^+ ions on the electrode surface.

$$C = \frac{\epsilon S}{4\pi kd} \quad (\text{Equation 1})$$

$$C = \frac{Q}{U} \quad (\text{Equation 2})$$

where C is the capacitance value, ϵ is the dielectric constant, S is the area directly opposite the capacitor pole plates, k is the electrostatic force constant, d is the distance between the capacitor pole plates, Q is the amount of charge carried by the capacitor, and U is the voltage value of the capacitor.

To verify the enhancement of the electric double layer by mica flakes, we conducted measurements of the capacitance of the electric double layer. Cyclic voltammetry (CV) scans of Ag nanoparticles, Ag-graphene, and Ag-mica were performed on the non-Faraday region at various scanning rates, as shown in Figure S8. By plotting the difference in charge/discharge current against the scanning rate, Figure 3D can be obtained. Calculating the slopes, we found that the capacitance values of electric double layer are 0.83 mF cm^{-2} , 0.81 mF cm^{-2} , and 2.01 mF cm^{-2} for Ag, Ag-graphene, and Ag-mica, respectively. The Ag nanoparticles and Ag-graphene have similar values of the electric double layer capacitance, whereas modification using mica flakes greatly increases the electric double layer capacitance, which is 2.4 times that of the initial Ag nanoparticles. This confirms our assumption that mica is able to enhance the electric double layer capacitance.

In situ attenuated total reflection Fourier transform infrared spectroscopy (ATR-FTIR) tests have been further utilized to explore the reaction intermediates. Figure 4A illustrates a schematic of the *in situ* ATR-FTIR spectroscopy, where the refracted light path passes through the silica column to detect the presence of reaction intermediates at the solid-liquid interface. This provides valuable evidence for understanding the reaction mechanism. To explore whether the increased capacitance value after mica flakes modification enhances the local CO_2 concentration, we compared the peak intensity at $2,345 \text{ cm}^{-1}$ between Ag nanoparticles and Ag-mica under an applied potential of -0.2 V vs. RHE . This particular peak corresponds to the stretching vibration of CO_2 molecules, and the single peak indicates the CO_2 dissolved in the electrolyte (Figure 4B).^{31,32} It is evident that the CO_2 peak intensity increases after mica flake modification, indicating that mica flakes can indeed enhance the local CO_2 concentration on the electrode surface. By verifying the design of our model, we have established that mica flakes within the electric double layer improve the capacitance, leading to an increased CO_2 concentration on the electrode surface. This enhancement facilitates the mass transfer process and enables higher current density to be achieved.

As depicted in Figure 4C, the peak located at $1,650 \text{ cm}^{-1}$ gradually strengthens as the applied potential becomes more negative, attributing to the C=O asymmetric stretching vibration of $^*\text{COOH}$ on Ag.³³ The linear adsorption of $^*\text{CO}$ located around $2,100 \text{ cm}^{-1}$ was also detected as the potential becomes more negative (Figure 4D).³⁴ It is noteworthy that these adsorption intermediates exhibit a shift in peak position with changing potential, a phenomenon known as the Stark effect. Considering that the conversion of CO_2 to $^*\text{COOH}$ involves one electron and one proton transfer, while the conversion to $^*\text{CO}$ requires two electrons and two protons, we can infer the pathway from CO_2 to CO as shown in Figure 4A. Initially, CO_2 is enriched and adsorbed onto the electrode surface. It then undergoes electron and proton transfer to convert into $^*\text{COOH}$. Subsequently, $^*\text{COOH}$ continues to be hydrodynamically reduced, transitioning to the adsorbed state of $^*\text{CO}$. Finally, CO detaches from the catalytic site and enters the gas phase, completing the reaction process.

Conclusions

The electrical double layer formed at the electrode-electrolyte interface has significant impacts on CO_2RR but has been barely acknowledged. In the present study we employed two-dimensional mica flakes to modify Ag nanoparticles to investigate the role of the electrical double layer. Following modification, the enhanced capacitance of the electrical double layer prompted K^+ ions aggregation and then resulted in substantial CO_2 enrichment. As a result, the activity of CO_2RR experienced a notable enhancement with high CO Faradaic efficiency of

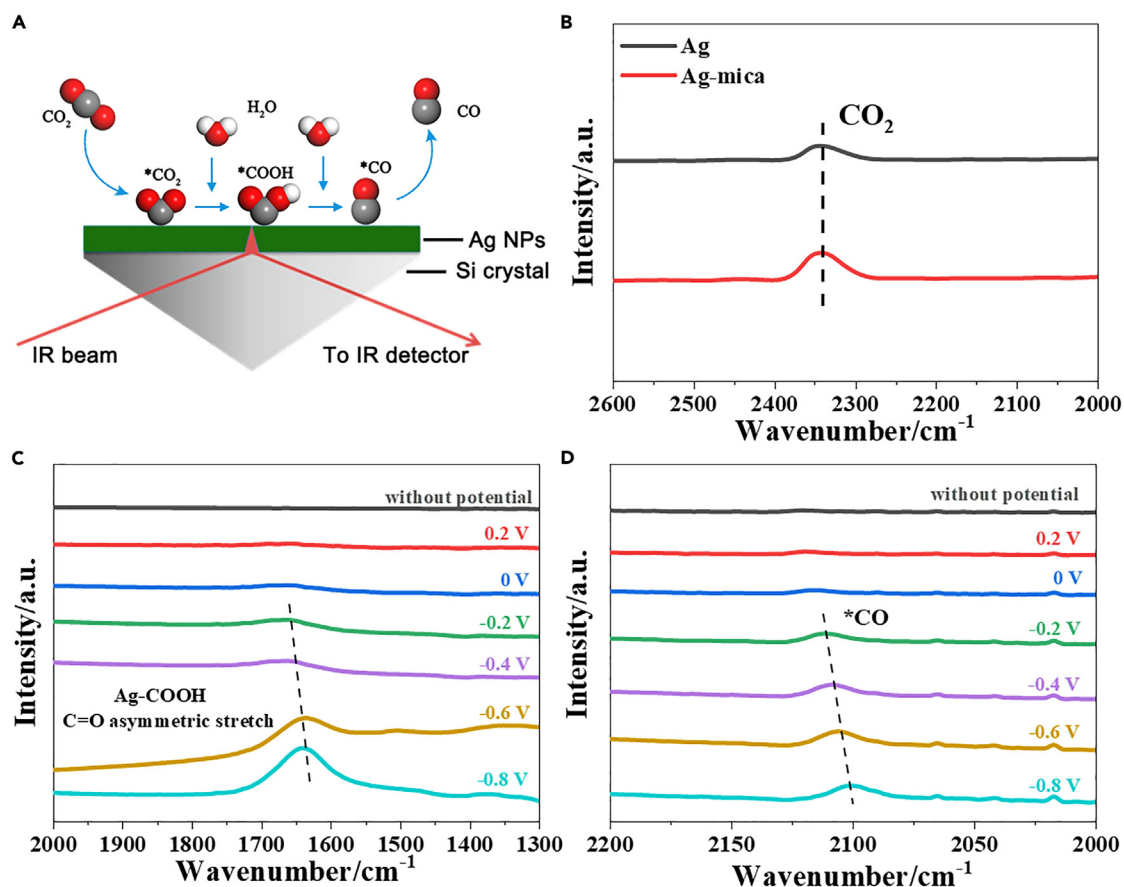


Figure 4. In situ ATR-FTIR investigation

(A) Schematic diagram of *in situ* ATR-FTIR for detection of intermediates.

(B) *In situ* ATR-FTIR spectra of Ag nanoparticles and Ag-mica at -0.2 V vs. RHE.

(C and D) *In situ* ATR-FTIR spectra of Ag-mica at different potentials.

98%. Our model not only provides a better understanding of the role of the electrical double layer but also serves as a reference for studying other electrocatalytic reactions.

Limitations of the study

The interfacial investigation is complicated, and future research that will focus on the electrode-electrolyte interface is required.

STAR★METHODS

Detailed methods are provided in the online version of this paper and include the following:

- KEY RESOURCES TABLE
- RESOURCE AVAILABILITY
 - Lead contact
 - Materials availability
 - Data and code availability
- METHOD DETAILS
 - Exfoliation of mica
 - Preparation of catalysts and electrodes
 - Characterizations
 - Electrochemical measurements
 - In-situ ATR-FTIR characterizations

SUPPLEMENTAL INFORMATION

Supplemental information can be found online at <https://doi.org/10.1016/j.isci.2024.109060>.

ACKNOWLEDGMENTS

The authors are grateful for the financial support from the National Nature Science Foundation of China (grant no. 22078232 and 21938008) and National Key Research and Development Program of China (grant no. 2023YFA1507900).

AUTHOR CONTRIBUTIONS

Q.F. and G.B. contributed equally. Conceptualization, Q.F. and S.Z.; methodology, Q.F. and G.B.; investigation, G.B., H.L., and X.C.; measurements, Q.F., G.B., Y.X., X.Z., and K.L.; writing – original draft, Q.F.; writing – review & editing, P.K., S.Z., and X.M.; funding acquisition, S.Z. and X.M.; supervision, S.Z. and X.M.

DECLARATION OF INTERESTS

The authors declare no competing interests.

Received: August 31, 2023

Revised: December 7, 2023

Accepted: January 25, 2024

Published: February 1, 2024

REFERENCES

1. Yan, T., Chen, X., Kumari, L., Lin, J., Li, M., Fan, Q., Chi, H., Meyer, T.J., Zhang, S., and Ma, X. (2023). Multiscale CO₂ electrocatalysis to C₂₊ products: Reaction mechanisms, catalyst design, and device fabrication. *Chem. Rev.* 123, 10530–10583.
2. Overa, S., Ko, B.H., Zhao, Y., and Jiao, F. (2022). Electrochemical approaches for CO₂ conversion to chemicals: A journey toward practical applications. *Acc. Chem. Res.* 55, 638–648.
3. Kuang, S., Su, Y., Li, M., Liu, H., Chuai, H., Chen, X., Hensen, E.J.M., Meyer, T.J., Zhang, S., and Ma, X. (2023). Asymmetrical electrohydrogenation of CO₂ to ethanol with copper-gold heterojunctions. *Proc. Natl. Acad. Sci. USA* 120, e2214175120.
4. Wang, H. (2022). Nanostructure@metal-organic frameworks (mofs) for catalytic carbon dioxide (CO₂) conversion in photocatalysis, electrocatalysis, and thermal catalysis. *Nano Res.* 15, 2834–2854.
5. Li, J., Sun, Y., and Zhang, Z. (2023). Revealing active Cu nanograins for electrocatalytic CO₂ reduction through operando studies. *SmartMat*, e1209. <https://doi.org/10.1002/smm2.1209>.
6. Zhang, S., Fan, Q., Xia, R., and Meyer, T.J. (2020). CO₂ reduction: From homogeneous to heterogeneous electrocatalysis. *Acc. Chem. Res.* 53, 255–264.
7. Yang, D., and Wang, X. (2022). 2D π -conjugated metal-organic frameworks for CO₂ electroreduction. *SmartMat* 3, 54–67.
8. Liu, H., Su, Y., Kuang, S., Hensen, E.J.M., Zhang, S., and Ma, X. (2021). Highly efficient CO₂ electrolysis within a wide operation window using octahedral tin oxide single crystals. *J. Mater. Chem. A* 9, 7848–7856.
9. Kuang, S., Li, M., Xia, R., Xing, L., Su, Y., Fan, Q., Liu, J., Hensen, E.J., Ma, X., and Zhang, S. (2020). Stable surface-anchored Cu nanocubes for CO₂ electroreduction to ethylene. *ACS Appl. Nano Mater.* 3, 8328–8334.
10. Kuang, S., Li, M., Chen, X., Chi, H., Lin, J., Hu, Z., Hu, S., Zhang, S., and Ma, X. (2023). Intermetallic cuau nanoalloy for stable electrochemical CO₂ reduction. *Chin. Chem. Lett.* 34, 108013.
11. Wang, H., Chuai, H., Chen, X., Lin, J., Zhang, S., and Ma, X. (2023). Self-supported porous carbon nanofibers decorated with single Ni atoms for efficient CO₂ electroreduction. *ACS Appl. Mater. Interfaces* 15, 1376–1383.
12. Bohra, D., Chaudhry, J.H., Burdyny, T., Pidko, E.A., and Smith, W.A. (2019). Modeling the electrical double layer to understand the reaction environment in a CO₂ electrocatalytic system. *Energy Environ. Sci.* 12, 3380–3389.
13. Fan, Q., Bao, G., Chen, X., Meng, Y., Zhang, S., and Ma, X. (2022). Iron nanoparticles tuned to catalyze CO₂ electroreduction in acidic solutions through chemical microenvironment engineering. *ACS Catal.* 12, 7517–7523.
14. Zang, D., Gao, X.J., Li, L., Wei, Y., and Wang, H. (2022). Confined interface engineering of self-supported Cu@N-doped graphene for electrocatalytic CO₂ reduction with enhanced selectivity towards ethanol. *Nano Res.* 15, 8872–8879.
15. Bockris, J.O.M., Devanathan, M.A.V., and MÜLLER, K. (1965). On the structure of charged interfaces. In *Electrochemistry*, J.A. Friend and F. Gutmann, eds. (Pergamon), pp. 832–863.
16. Aikens, D.A. (1983). Electrochemical methods, fundamentals and applications. *J. Chem. Educ.* 60, A25.
17. Parsons, R. (1990). The electrical double layer: Recent experimental and theoretical developments. *Chem. Rev.* 90, 813–826.
18. Haid, R.W., Ding, X., Sarpey, T.K., Bandarenka, A.S., and Garlyyev, B. (2022). Exploration of the electrical double-layer structure: Influence of electrolyte components on the double-layer capacitance and potential of maximum entropy. *Curr. Opin. Electrochem.* 32, 100882.
19. Dunwell, M., Yan, Y., and Xu, B. (2018). Understanding the influence of the electrochemical double-layer on heterogeneous electrochemical reactions. *Curr. Opin. Chem. Eng.* 20, 151–158.
20. Gu, J., Liu, S., Ni, W., Ren, W., Haussener, S., and Hu, X. (2022). Modulating electric field distribution by alkali cations for CO₂ electroreduction in strongly acidic medium. *Nat. Catal.* 5, 268–276.
21. Li, P., Jiang, Y., Hu, Y., Men, Y., Liu, Y., Cai, W., and Chen, S. (2022). Hydrogen bond network connectivity in the electric double layer dominates the kinetic pH effect in hydrogen electrocatalysis on pt. *Nat. Catal.* 5, 900–911.
22. Shin, S.-J., Kim, D.H., Bae, G., Ringe, S., Choi, H., Lim, H.-K., Choi, C.H., and Kim, H. (2022). On the importance of the electric double layer structure in aqueous electrocatalysis. *Nat. Commun.* 13, 174.
23. Resasco, J., Chen, L.D., Clark, E., Tsai, C., Hahn, C., Jaramillo, T.F., Chan, K., and Bell, A.T. (2017). Promoter effects of alkali metal cations on the electrochemical reduction of carbon dioxide. *J. Am. Chem. Soc.* 139, 11277–11287.
24. Verma, S., Lu, X., Ma, S., Masel, R.I., and Kenis, P.J.A. (2016). The effect of electrolyte composition on the electroreduction of CO₂ to CO on Ag based gas diffusion electrodes. *Phys. Chem. Chem. Phys.* 18, 7075–7084.
25. Singh, M.R., Kwon, Y., Lum, Y., Ager, J.W., III, and Bell, A.T. (2016). Hydrolysis of electrolyte cations enhances the electrochemical reduction of CO₂ over Ag and Cu. *J. Am. Chem. Soc.* 138, 13006–13012.
26. Zhang, X., He, Y., Li, R., Dong, H., and Hu, W. (2016). 2D mica crystal as electret in organic field-effect transistors for multistate memory. *Adv. Mater.* 28, 3755–3760.
27. Pan, X.-F., Gao, H.-L., Lu, Y., Wu, C.-Y., Wu, Y.-D., Wang, X.-Y., Pan, Z.-Q., Dong, L., Song, Y.-H., Cong, H.-P., and Yu, S.H. (2018). Transforming ground mica into high-performance biomimetic polymeric mica film. *Nat. Commun.* 9, 2974.

28. Yen, M., Bitla, Y., and Chu, Y.-H. (2019). Van der waals heteroepitaxy on muscovite. *Mater. Chem. Phys.* *234*, 185–195.
29. Liu, M., Pang, Y., Zhang, B., De Luna, P., Voznyy, O., Xu, J., Zheng, X., Dinh, C.T., Fan, F., Cao, C., et al. (2016). Enhanced electrocatalytic CO₂ reduction via field-induced reagent concentration. *Nature* *537*, 382–386.
30. Garcia de Arquer, F.P., Dinh, C.-T., Ozden, A., Wicks, J., McCallum, C., Kirmani, A.R., Nam, D.-H., Gabardo, C., Seifitokaldani, A., Wang, X., et al. (2020). CO₂ electrolysis to multicarbon products at activities greater than 1 a cm⁻². *Science* *367*, 661–666.
31. Dou, T., Du, J., He, J., Wang, Y., Zhao, X., Zhang, F., and Lei, X. (2022). Sulfurization-derived Cu⁰–Cu⁺ sites for electrochemical CO₂ reduction to ethanol. *J. Power Sources* *533*, 231393.
32. Kas, R., Ayemoba, O., Firet, N.J., Middelkoop, J., Smith, W.A., and Cuesta, A. (2019). In-situ infrared spectroscopy applied to the study of the electrocatalytic reduction of CO₂: Theory, practice and challenges. *ChemPhysChem* *20*, 2904–2925.
33. Firet, N.J., and Smith, W.A. (2017). Probing the reaction mechanism of CO₂ electroreduction over Ag films via operando infrared spectroscopy. *ACS Catal.* *7*, 606–612.
34. Bai, H., Cheng, T., Li, S., Zhou, Z., Yang, H., Li, J., Xie, M., Ye, J., Ji, Y., Li, Y., et al. (2021). Controllable CO adsorption determines ethylene and methane productions from CO₂ electroreduction. *Sci. Bull.* *66*, 62–68.

STAR★METHODS

KEY RESOURCES TABLE

REAGENT or RESOURCE	SOURCE	IDENTIFIER
Chemicals, peptides, and recombinant proteins		
Silver nitrate	Shanghai Aladdin Biochemical Technology Co., Ltd.	CAS#7761-88-8
Sodium citrate	Shanghai Aladdin Biochemical Technology Co., Ltd.	CAS#6132-04-3
Sodium borohydride	Shanghai Aladdin Biochemical Technology Co., Ltd.	CAS#16940-66-2
Nafion	Shanghai Aladdin Biochemical Technology Co., Ltd.	CAS#31175-20-9
Mica	Goode EIS (Suzhou) Corp., Ltd.	CAS#12001-26-2
Sodium chloride	Shanghai Macklin Biochemical Technology Co., Ltd.	CAS#7647-14-5
potassium chloride	Shanghai Macklin Biochemical Technology Co., Ltd.	CAS#7447-40-7
potassium bicarbonate	Shanghai Macklin Biochemical Technology Co., Ltd.	CAS#298-14-6
Graphene	Nanjing XFNANO Materials Tech Co., Ltd.	CAS#1034343-98-0
Carbon dioxide	Air Liquide China Holding Co., Ltd.	CAS#124-38-9
Argon	Air Liquide China Holding Co., Ltd.	CAS#7440-37-1

RESOURCE AVAILABILITY

Lead contact

Further information and requests for resources and reagents should be directed to and will be fulfilled by the lead contact, Sheng Zhang (sheng.zhang@tju.edu.cn).

Materials availability

No new reagents were created in the presented research.

Data and code availability

- All data reported in this paper will be shared by the [lead contact](#) upon request.
- This paper does not report original code.
- Any additional information required to reanalyze the data reported in this paper is available from the [lead contact](#) upon request.

METHOD DETAILS

Exfoliation of mica

Mica flakes were prepared by bulk mica through ultrasonic assisted liquid-phase exfoliation combined with ion exchange. Initially, 2 g of commercial white mica was added to 400 mL of saturated NaCl solution, condensed and refluxed at 120°C for 48 h, followed by ultrasonication for 3 h for exfoliation. Subsequently, the dispersion was centrifuged at 3000 rpm for 15 min to obtain the supernatant, and the supernatant was filtered to obtain the solid and washed with deionised water. The obtained solid was immersed in 200 mL of 2 M KCl solution for 3 h for ion exchange. Following that, diafiltration and additional washing with deionised water were conducted to remove any excess ions. Finally, the mica flakes were dried at 90°C overnight to obtain the desired product.

Preparation of catalysts and electrodes

Ag nanoparticles were prepared by simple liquid phase reduction of sodium borohydride. Firstly, 0.4 mmol of sodium citrate was dissolved in 100 mL of deionised water and Ar gas was passed for 30 min to remove the dissolved air from the water. Subsequently, 0.4 mmol of AgNO₃ was added and stirred to dissolve and continuously passed through Ar gas. 0.6 mmol of sodium borohydride was dissolved in 10 mL of water and loaded into a constant pressure dropping funnel to drop into a mixed solution of silver nitrate and sodium citrate and allowed to finish dropping within 8 min. After standing for 5 min, centrifugation at 9000 rpm for 5 min was performed for separation and washed three times with the mixture of deionised water and ethanol. Finally, Ag nanoparticles were dried at 60°C for 5 h.

Ag nanoparticles were configured as a catalyst slurry drop-coated onto a glassy carbon electrode and modified with mica flakes. The electrode surface was first polished with 0.3 μm and 0.05 μm Al₂O₃ powders, subsequently cleaned by sonication in a mixture of deionised water and ethanol, and blown dry for use. 10 mg of sample powder was weighed and dispersed in 5 mL of isopropanol, and 10 μL of 5 wt% Nafion

solution was added as a binder, which was sonicated for 1 h to form a homogeneous catalyst slurry. 5 μL of catalyst slurry was accurately pipetted with a pipette gun and applied dropwise onto a 6 mm glassy carbon electrode, and the above operation was repeated 7 times after drying.

The mica flakes were configured into a 0.2 mg mL^{-1} suspension of isopropanol, dispersed uniformly by ultrasonication. 6 μL of the above slurry was applied dropwise to the above glassy carbon electrode, and then left to dry. For comparison, commercial graphene was also used to carry out the modification of the electrodes in the same way as the mica flakes.

Characterizations

X-ray powder diffraction (XRD) was performed with a D8 Advance diffractometer (Bruker) equipped with a $\text{Cu K}\alpha$ radiation. X-ray photoelectron spectroscopy (XPS) experiments were carried out using photoelectron spectrometer (K-Alpha+) with a monochromatic Al $\text{K}\alpha$ X-ray (1486.6 eV) source. All spectra were calibrated according to the C 1s binding energy at 284.8 eV. Scanning electron microscopy was carried out using a field emission microscope (SEM, S-4800) operated at 20 kV. Transmission electron microscope (TEM) was conducted using JEOL-2100F and JEOL ARM200F microscope. TEM samples were prepared by depositing a droplet of suspension onto a Cu grid coated with a Lacey Carbon film.

Electrochemical measurements

Controlled potential electrolysis of CO_2 was tested in a custom-made gas-tight H-cell system, which was separated by a Nafion 117 membrane. Pt wire and Ag/AgCl electrodes (filled with saturated KCl aqueous solution) were used as counter electrode and reference electrode, respectively. The potentials were controlled by an electrochemical working station (CHI 760E, Shanghai CH Instruments Co., China). All potentials in this study were measured against the Ag/AgCl reference electrode and converted to the RHE reference scale by

$$E \text{ (vs. RHE)} = E \text{ (vs. Ag / AgCl)} + 0.21 \text{ V} + 0.0591 \times \text{pH}$$

Electrocatalytic CO_2 reduction was conducted in CO_2 -saturated KHCO_3 solution (0.1 M) at room temperature and atmospheric pressure. CO_2 was purged into the KHCO_3 solution for at least 30 min to remove residual air in the reservoir. For the faradaic efficiency analysis, gas products were detected by gas chromatograph (GC, Agilent 7890B) and liquid products were characterized by ^1H NMR on AVANCE IIIITM HD 400 MHz NanoBAY.

Faradaic efficiency is based on the definition as follow:

$$\text{FE} = Q_{\text{CO}}/Q_{\text{total}} = (Z \times n \times F)/Q_{\text{total}}$$

where Z is the number of electrons transferred ($Z = 2$ for CO and H_2 production), n the number of moles for a given product, F Faraday's constant (96485 C mol^{-1}), Q_{total} all the charge passed throughout the electrolysis process (measured by calculating the curve area of current density vs. time plot). CO and H_2 mole fractions of injected samples were calculated based on GC calibration curve. The error bars represent two repeated electrolysis with different batches of catalysts.

The electrical double layer capacitance was estimated based on the CV results under the potential windows of 0.4 V \sim 0.7 V (vs. RHE). Electrochemical impedance spectroscopy (EIS) measurements were carried out by applying an AC voltage with 5 mV amplitude in a frequency range from 0.1 to 10^6 Hz.

In-situ ATR-FTIR characterizations

The operando FTIR measurements were performed with Thermo Fisher Nicolet iS50. The measurements were conducted in a home-made 3-electrode spectroelectro-chemical cell. Ag/AgCl electrode and Pt wire were used as the reference and counter electrode, respectively. Silica pillared sprayed gold for 50 S, then catalyst ink dropped on silica pillared as working electrode. During each experiment, CO_2 was bubbled through the electrolyte. A background spectrum was then taken without potential. To test gaseous CO_2 , the accumulation time was 10 s. The spectra depended on potentials were obtained by applying single potential steps, and collected after running for 90s.